Ultrasonics Sonochemistry 88 (2022) 106069

Contents lists available at ScienceDirect

Ultrasonics Sonochemistry

journal homepage: www.elsevier.com/locate/ultson

The physical, mechanical, thermal and barrier properties of starch nanoparticle (SNP)/polyurethane (PU) nanocomposite films synthesised by an ultrasound-assisted process

Vikas S. Hakke [a], Vividha K. Landge [a], Shirish H. Sonawane [a,*], G. Uday Bhaskar Babu [a], Muthupandian Ashokkumar [b], Erico M. M. Flores [c]

[a] Department of Chemical Engineering, National Institute of Technology Warangal, Warangal 506004, Telangana State, India
[b] School of Chemistry, University of Melbourne, VIC 3010, Australia
[c] Department of Chemistry, Federal University of Santa Maria, 97105-900 Santa Maria, RS, Brazil

ARTICLE INFO

Keywords:
Starch nanoparticles
Nanofiller
Mechanical strength, Water vapor permeability, Bacterial barrier
Ultrasound treatment

ABSTRACT

This article reports on the ultrasound-assisted acid hydrolysis for the synthesis and evaluation of starch nanoparticles (SNP) as nanofillers to improve the physical, mechanical, thermal, and barrier properties of polyurethane (PU) films. During the ultrasonic irradiation, dropwise addition of 0.25 mol L^{-1} H_2SO_4 was carried out to the starch dispersion for the preparation of SNPs. The synthesized SNPs were blended uniformly within the PU matrix using ultrasonic irradiation (20 kHz, 220 W pulse mode). The temperature was kept constant during the synthesis (4 °C). The nanocomposite coating films were made with a regulated thickness using the casting method. The effect of SNP content (wt%) in nanocomposite coating films on various properties such as morphology, water vapour permeability (WVP), glass transition temperature (Tg), microbial barrier, and mechanical properties was studied. The addition of SNP to the PU matrix increased the roughness of the surface, and Tg by 7 °C, lowering WVP by 60% compared to the PU film without the addition of SNP. As the SNP concentration was increased, the opacity of the film increased. The reinforcement of the SNP in the PU matrix enhanced the microbial barrier of the film by 99.9%, with the optimal content of SNP being 5%. Improvement in the toughness and barrier properties was observed with an increase in the SNP content of the film.

1. Introduction

The widespread use of petroleum based polymeric films for various applications generates a huge number of environmental pollutants. The limited petroleum resources and non-availability of techniques for the complete disposal of synthetic polymers make the use of such synthetic polymers dangerous and harmful to the environment. As a result, there is a pressing need to create ecologically benign and biodegradable polymers. Waste generated from agriculture, marine, and food industry may be used as a renewable resource for the synthesis of degradable natural polymers [1]. Biopolymers such as chitosan [2], protein [3], and cellulose [4] have been successfully blended with polyvinyl alcohol (PVA) [5] and glycerol [6] for the preparation of polymers that degrade faster than synthetic polymers.

Starch and its derivatives have gained considerable attention because of their abundance in nature and wide potential for various applications in food industries, polymer nanocomposite coatings, and films [7]. The use of ultrasound (US) to help modify the structure of starch granules has been reported. During the cavitation event, cohesive forces were created in the liquid to cause disturbance in the liquid. Ultrasonic irradiation creates cavities that collapse resulting in localized high pressures and temperatures, leading to the formation of radicals. Furthermore, the generation of shock waves during bubble collapse significantly improves mass transfer and emulsification processes, two critical factors that influence reaction rates and improve reactant deagglomeration. The green chemistry approach for the synthesis of biomass-based nanoparticles using US can bring some advantages as compared to larger reactors as it can be eco-friendly, non-thermal technology [10,11]. The high intensity irradiation of US may cause the destruction of microcapsules in the solution. Inui et al. [12] studied the phenomenon of destruction of microcapsules of starch under US irradiation. The shear stress induced due to the collapse of bubbles in

* Corresponding author.
E-mail address: shirish@nitw.ac.in (S.H. Sonawane).

https://doi.org/10.1016/j.ultsonch.2022.106069
Received 2 April 2022; Received in revised form 5 June 2022; Accepted 13 June 2022
Available online 17 June 2022

solution is one of the reasons for the physical destruction of structure of starch [12]. Haaj et al. [13] found that at high intensity US irradiation (24 kHz, horn tip diameter 13 mm, 170 W) physically damage the crystalline structure of starch. They also reported the higher yield for the synthesis of SNP as compared to the conventional acid hydrolysis method. Zhou et al. [14] reported acid vapour hydrolysis assisted with US irradiation (20–25 kHz) for the synthesis of elliptical shaped SNP. However, they also found that gelatinization temperature and overall crystallinity of synthesized SNP were lower than the native starch granules.

Ultrasonic irradiation can easily achieve a uniform distribution of nanoparticles. Shear forces caused by shock waves, collisional impact on particle surface, and cavitation induced by the US pressure gradient are among the key characteristics determining nanoparticle distribution. Girard et al. [15] reported the effect of sonication on the dispersion of cellulose nanocrystals. They discovered that raising the energy level resulted in a well-dispersed suspension As expected, by increasing the time of ultra-sonication, more mixing cycles can be done and the process can be accelerated. However, the multiple particle interactions and the higher local concentration of nanoparticles can overcome the dispersion energy induced by US. Sumitomo et al. [16] reported a comparative study between the dispersion developed by mechanical stirring and US irradiation. They found that US is much more efficient to achieve a well dispersed solution as compared to mechanical agitation. As the irradiation period increased, the viscosity and average size of the aggregates in suspension decreased [17].

Starch is hydrophilic in nature, it also shows poor water vapour, oxygen and bacterial passage barrier properties. For the application of starch-based polymer films for wider applications, it is necessary to overcome these limitations. The synthesis of starch-based polymeric films using various plasticizers has been reported in the literature [18]. The addition of plasticizers such as glycerol [19,20], formamide [21], urea, sucrose, and sorbitol [22] effectively enhances the mechanical properties of polymer film such as tensile strength, modulus of elasticity, break-even point. These modified starch-based nanocomposite polymer films are sensitive to moisture and heat, due to the hydrophilicity of the starch granules [12]. Therefore, the investigation of strategies to improve the properties of starch-based polymer films are still necessary. The blending of proteins with starch brings hydrophobicity in the starch-based polymer films as well as increases the tensile strength of the polymer film [3].

SNPs can be used as nanofillers in the continuous matrix of other natural or synthetic polymers for the production of packaging films [7,23]. The reinforcement of SNPs not only improves the mechanical and physical properties but also the biodegradability of the host polymer matrix. An effective reduction in water vapour and oxygen permeability of rubber latex was successfully demonstrated through blending of SNPs with natural rubber latex by Angellier et al. [24]. Concha et al. [25] found a 50% increase in the relative crystallinity of granules due to a reduction of starch granule size. This rise in the crystallinity of starch granule in SNPs provides strength and increases the rigidity of the host polymer [26].

Polyurethane (PU) is the most popular polymer used in various products and applications owing to its low cost and low toxicity. However, poor wear and tear resistance, optical properties, and lower hardness are the drawbacks of PU based films. The modification in PU based films has been studied and demonstrated by various blending materials such as vegetable oil [27], coumarin derivatives [28], nano-silver [29], cellulose nanocrystals [30], etc. This results in the improvement of the mechanical, physical, and chemical properties of the PU films. Zhang et al. [31] used thermoplastic PU and blended it with the lactic acid to achieve more interfacial compatibility with PU. They found enrichment in the mechanical properties of the PU based polylactic acid film. In another research, Zhang et al. [32] reported the improvement of mechanical properties and optical properties of PU based films by the addition of monocrystalline cellulose. They found that the variation in hardness is only 1.5% but the properties like abrasion resistance of PU based films with monocrystalline cellulose was enhanced by 60%, a good achievement for coating application. Another successful attempt reported by Lu et al. [33] was the blending of glycerol plasticized starch granules with PU. The reported PU film presented enhanced surface area, hydrophobicity, and water resistance. However, the toughness of the film was not affected. Yazdi et al. [34] modified the PU matrix with the addition of multi-walled carbon nanotubes. The authors reported enhancement in modulus of elasticity and tensile strength of the PU film modified with multi-walled carbon nanotubes.

The commercially available water-born PU has a wide range of applications, starting from polymer barrier coating for food, decorative, protective coatings to the PU foam. The PU polymer structure is adaptive and easily accommodates/compatible with the filler material in the suspension. Though, starch is abundantly found, the nano starch synthesis and applications are not well explored. The abundantly available starch and its conversion to the nanoscale can be achieved with intensified ultrasound assisted acid hydrolysis. Further, the PU used is a water based resin, which is environmental friendly and can be used for coatings.

To the best of our knowledge, a few studies have explored the modification of PU with SNPs. In our previous report [35], we demonstrated the preparation of SNPs through ultrasound assisted acid hydrolysis. It was observed that, in the ultrasonically treated starch granules, the lower size as well as a narrower particle size distribution (PSD) were observed in a very short time as compared to other particle size reduction methods. However, the morphology of the produced SNPs was also altered from a plate-like structure to an oval shape under ultrasonic irradiation [36]. The acid hydrolysis assisted with ultrasonic irradiation enhances hydrolysis rate with the available starch granular surface. This rise in acid hydrolysis produces the lower particle size of starch granules at the reaction termination [25,37]. The major advantage of the ultrasound assisted acid hydrolysis is that due to shearing action and improved diffusion of acid inside the native starch there is reduction in particle size of the SNPs. Which is not observed in the conventional acid hydrolysis process. The obtained nanocrystals of starch were used as nanofillers and distributed uniformly in the PU matrix with US assistance.

In the present work, the synthesis and improvement in dispersion of SNP in a PU matrix using the ultrasonic irradiation has been reported. The ultrasonic irradiation enhances the dispersion of SNP during mixing (5, 10 20, 30 wt%) with the PU solution. The fabrication of SNP-PU nanocomposite films and their performance against the transmission of microorganisms and water vapor were investigated. These films have also been analysed for thermal and mechanical strength using standard characterization methods. It is observed that ultrasound assisted acid hydrolysis shows lower particle size of SNPs compared to conventional synthesis process, hence there is improved performance which is due to increase in the local crystallinity.

2. Materials and process for the synthesis of SNP-PU nanocomposite films.

2.1. Materials.

Analytical grade maize corn starch (29.1 ± 1.07% amylose content) and H_2SO_4 were purchased from Alfa-Aesar Pvt. Ltd., India. The PU resin was purchased from Merck Pvt. Ltd., India. Vacuum filtration was used for the separation of hydrolyzed starch. All the chemicals were used as supplied, and deionized (DI) water was used for all the stock solutions preparation.

2.2. Ultrasound synthesis of starch nanoparticles and dispersion of SNP in PU solution.

Synthesis of SNPs and dispersion of SNPs was carried out using

ultrasound assisted method. Maize corn starch powder (5 g) was dispersed in DI water at a temperature of 4 °C. The uniform dispersion of starch grains in DI water was achieved with continuous stirring (250 rpm). The starch dispersion was sonicated with the help of probe (20 mm diameter) sonicator used in glass beaker surrounded with cooling water (Dakshin Mumbai India 20 kHz,120 W) at 225 V and 0.9 A in pulse mode (3 s on and 2 s off). During the ultrasonic irradiation, dropwise addition of 0.25 mol L^{-1} H_2SO_4 was made to the starch dispersion. The temperature was kept steady during the whole process (4 °C). The starch solution was maintained overnight in a shaker after 45 min of sonication. A two-stage centrifugation was used to separate the produced SNPs. The centrifuged SNP was dried in a vacuum desiccator before being utilized in the next step of the process.

The yield of SNP synthesized was calculated on the basis of the weight of separated nano granules of starch after drying. In the first stage of centrifugation (1000 rpm, 5 min). The coarser micron-sized starch granules are observed to settle down at the bottom, and nanoparticles still remain in the supernatant. In the second stage, the supernatant from the first stage is centrifuged for 5 min at 9500 rpm. At this high speed, the nanoparticles from suspension gets settled down at the bottom of the centrifuge tube, which were then dried and the weight was noted for the calculation of the yield of SNP.

The dispersion of 205 mg of SNP in deionised water (50 mL, 200 mL glass beaker) was achieved with the 5 min US irradiation in pulse mode (3 s on and 2 s off). The pulse mode was utilized to control the temperature of suspension. To enhance the easy interaction and dispersion of SNP in PU solution, the SNP was initially dispersed in DI water to adjust the viscosity for nanocomposite film preparation to apply on substrate. The dispersion of SNP in solution of PU was accomplished via 20 kHz sonication (5 min) at temperature of 20 °C. The well dispersed SNP-PU nanocomposite suspension than used for next process of thin sheet preparation.

2.3. Casting of nanocomposite film.

The uniformly blended mixture of SNP and PU was exploited for the synthesis of films through the casting technique. The 200 μm thickness of the nanocomposite sheets of well dispersed SNPs in PU solution was achieved using stainless steel (SS) film applicator 9031 (Samriddhi International Inc, Mumbai India). The produced nanocomposite thin sheets were then dried with the help of vacuum oven (VT 6025, Thermo Fisher Scientific India Pvt. Ltd.). Films of PU with SNP of 5, 10, 20, and 30% (wt) were synthesized and examined for variation in properties such as mechanical property, transmission resistance to bacteria, and water vapor permeability (WVP) at different temperatures. The 5% (wt) SNP is blended with the PU solution with the help of ultrasonic irradiation. This suspension is used to synthesize the nanocomposite film denoted as SP1. The different amounts of SNP in the PU solution are 10% (SP2), 20% (SP3), and 30% (SP3). These were made and stored in the desiccator to keep them away from getting wet and contaminated by bacteria.

The film applicator was used for the synthesis of films with uniform-thickness. The thickness of the film was verified by the digital thickness measurement device from the coating thickness gauge PCE-CT 80 (PCE Instruments UK). The random checks at different points confirm that the film's thickness was the same everywhere.

2.4. Analysis of nanocomposite films.

2.4.1. Morphological study of nanocomposite SNP-PU films.

Field emission scanning electron microscope (FESEM) (Gemini 500, M/s Carl Zeiss) was used to examine the morphology of films. FESEM cross-sectional views of the film verified a consistent distribution of SNPs. Malvern particle size analyser (Malvern, UK) was used to measure the produced starch granules particle size.

2.4.2. Thermophysical property analysis of thin films.

Thermogravimetric analysis (TGA) was used to estimate the glass transition temperatures (Tg) of the films and the perfect thermal resistance. The TGA studies were performed on the Perkin-Elmer instrument (TGA 8000, USA) under a nitrogen environment to demonstrate the thermdao-physical behaviour of nanocomposite film. An automated Mettler balance was used to weigh 6 samples of the thin films with a weight of about 5 mg was introduced in the pans. A fast press was used to seal the pan after it was put on a spacer insert. The reference was an empty pan with a cover that was sealed to provide a sufficient heat capacity. The film was tested three times and TGA was carried out at a heating rate of 5 °C min^{-1} from 25 to 350 °C with nitrogen gas flowing at a rate of 60 mL min^{-1}. The enthalpy change (ΔH) was calculated using the weight of the film and represented as J g^{-1} of dry matter.

2.4.3. Mechanical property analysis of nanocomposite SNP-PU films.

The mechanical characteristics of the film were determined using the Universal Testing Machine (UTM) T 150 tensile tester (KLA, India) as per the ASTM D 882 [38] standard test methods. The specimen (100 mm length × 3 mm thickness × 20 mm breadth) was taken in a tensile machine to determine the elongation (% E), and the tensile strength (TS) for the film with the constant crosshead speed of 5 mm/min.

$$\%\ \text{elongation}\ (\%\,\text{E}) = \frac{(L_f - L_i)}{L_i}\ \text{X}\ 100 \tag{1}$$

L_f is the final length of sample while L_i is the initial length of sample.

2.4.4. UV–visible spectrophotometry for the light transmittance and opacity.

UV–vis-NIR spectrophotometer (Cary 5000, Agilent technologies, USA) was used to observe the UV–Vis response of the SNP-PU nanocomposite film. The transmission (%T) was noted for different samples considering virgin PU film as the baseline. The individual component transmittance at 600 nm wavelength was noted. Lambert-Beer's equation was used to convert transmittance observation in absorbance. The opacity of films was calculated by, $Opacity = \frac{abs_{600}}{X}$; where X is the thickness of thin-film in mm.

2.4.5. Determination of bacterial passage through synthesized SNP-PU nanocomposite films.

To understand whether the films allowed the passage of bacteria, the following experiment was carried out. Six sterilized conical flasks were taken and 20 mL sterilized Luria-Bertani broth media was added to each of them. The mouth of the conical flasks was tightly sealed using the films and exposed to the environment for 24 h. One flask was left unsealed to act as a control. After exposure for 24 h, the conical flasks were incubated at 37 °C for 24 h at 180 rpm. Following this, the absorbance of the culture was measured at 600 nm using a spectrometer (UV-1800 model, Shimadzu Analytical Pvt. Ltd., India). The cultures were then diluted and spread plated on Luria-Bertani agar plates. These plates were maintained at 37 °C for 12 h and the bacterial count in each agar plate was determined. The total bacterial count in each conical flask was calculated after considering the dilution factor. All experiments were performed in triplicate and the standard error of the mean was calculated.

2.4.6. Determination of water vapor permeability of nanocomposite film.

WVP tests were conducted using ASTM (1996) [26] method E96 with some modifications. Each film sample was sealed over a circular opening of a cylindrical vessel of an opening diameter of 6 cm. The cylindrical vessel was filled with water. The desiccator temperature was monitored by a water-heated thermostat (28 °C, 35 °C, 40 °C) and a temperature measuring indicator was placed inside the desiccator to monitor the temperature. To maintain the relative humidity (RH) across the film, anhydrous calcium chloride (75% RH) was placed in the desiccator. The

effect of temperature on the water vapour transmission from inside vessel to outside through the film was observed. The weight difference of vessel and cross-sectional area of film were used to calculate the water vapours permission rate (WVPR). After the attainment of steady-state (about 32 h), the WVP (g/Pa.s.m) was calculated as WVP = [WVPR/S ($R_1 - R_2$)] d, where S is the saturation vapor pressure of water (Pa) at the test temperature, R_1 is the RH in the desiccator, R_2 is the RH in the permeation cell and d is the film thickness (m).

2.4.7. Oxygen barrier performance of the SNP-PU nanocomposite film.

To measure the oxygen permeability of thin films, samples of thin films were examined using the ASTM 3985 standard test [39]. By inserting the test sample in one of the chambers, permeation cells were employed to create a barrier between two compartments. Both chambers were entirely decommissioned. Following that, one compartment was filled with nitrogen, while the other was filled with oxygen. Because of the barrier, oxygen may seep into the nitrogen carrier gas and be transported to the colorimetric detector, causing an electrical current to flow. The signal's strength was related to the quantity of oxygen flowing into the detector.

3. Result and discussion

Ultrasound probe reactor was used for the acid hydrolysis of the starch granules using H_2SO_4 (0.25 mol L^{-1}). The overall power dissipation to the suspension of starch granules and water was 202 W for 100 mL suspension with 40% power setting (power density = 0.808 W cm^{-3}). In our previously reported work, we conduct the ultrasound assisted acid hydrolysis with the different acid concentration and found that with the same power index and other operating conditions at 0.25 M acid concentration, synthesized starch granules shows uniform particle size distribution with overall minimal particle size. Due to which 0.25 mol L^{-1} H_2SO_4 was used in the present study to prepare SNPs[35].

Fig. 1 shows the effect of irradiation time on the granular size of the starch. The results demonstrate that the rapid penetration of acid molecules through the cell membrane and the intensification of mass transport of acid molecules through the surrounding film of starch molecules are induced due to the physical effects caused by ultrasound on the surface of the starch particles. Another possibility may be associated with the surface pore volume associated with the starch particles. These pores of starch granules could be occupied by air molecules. It is also possible that trapped air pockets within the starch particles could expand under negative acoustic pressure and this could rupture the cell walls of starch particles [25].

According to the two-film theory of mass transfer, for the particles suspended in the solution, two layers of film induce the overall mass transfer resistance [40]. This mass transfer resistance offered by the two films generated surrounding the starch granules must be overcome by the acid molecules to reach the starch surface for the initiation of acid hydrolysis. The breakdown of these two films was achieved during ultrasonic irradiation. This phenomenon helps acid molecules to reach the starch surface rapidly as compared to the conventional acid hydrolysis method [25]. The impingement and permeation of acid molecules in the starch granules is aided by ultrasonic irradiation, which increases the acid hydrolysis rate [25].

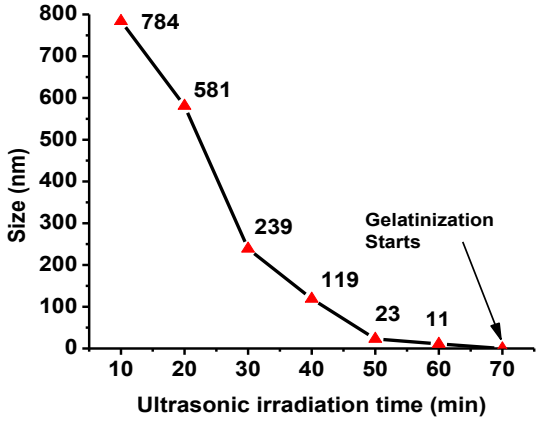

Fig 1. Effect of ultrasonic irradiation time on the starch granular size.

The observed particle size data indicate that as the irradiation time increases, the resistive strength of starch granules against acid hydrolysis reduces leading to a breakdown of starch granules. The high power density ultrasonic irradiation develops higher number of cavities during the mild acid hydrolysis of starch using 0.25 mol L^{-1} H_2SO_4. This results in the higher number of collapses in the suspension. Probably, the generated micro jets in solution leads to the local high pressure drop which enhances the physical destruction of complex structure of starch granules. Further, the shear forces generated by cavitation process may cause cracks on the surface of starch granules. During this physical destruction/pitting on the surface, the amorphous zone where the amylose and amylopectin are randomly present gets exposed to the mild acid. The branched α-1,4-d-glucopyranose (amylopectin) reacts with 0.25 mol L^{-1} H_2SO_4 solution producing a complex gel-like highly viscous suspension that is dispersed in the solution. This degradation of the mass of starch granule leads to the reduction in its particles size. The longer time of ultrasonic exposure results in higher number of random collapses at or near to surface of starch granules. The complex structure of the product generated from hydrolysis diminishes the presence of crystalline structure at higher exposure time. The phenomenon of gelatinization was observed at longer time exposures of ultrasonic irradiation. The yield of synthesized SNP with the proposed ultrasound assisted acid hydrolysis was found to be 43% with an average PSD below 50 nm. The Change et al. [41] synthesized SNP with vacuum cold plasma followed by the ultrasonic irradiation and have reported the 87% of yield of SNP with particle size of about 500 nm. The proposed process yields more than Dai et al. [42] where they experimented with ball milling assisted acid hydrolysis of starch and achieved a yield of SNP of about 19.3% for PSD of about 50 nm.

The amorphous part of starch due to random packaging of amylose and amylopectin shows higher reaction kinetics with the mild acid environment than that of the crystalline compact packaging section of the starch granule structure. The starch hydrocarbon in the crystalline part of granule shows higher resistance for the hydrolysis. The physical forces generated due to acoustic cavitation facilitate the contact between acid and the amorphous part of the starch granule [13]. This enhances the rate of hydrolysis and reduces the granular size. A more uniform distribution of SNP nanofiller in the PU matrix could also be achieved by using ultrasound irradiation. The effective mixing of PU results in a homogenous distribution of SNPs in the film as shown in Fig. 2.

3.1. Morphological studies of SNP-PU nanocomposite films.

FESEM images in Fig. 2 show the cross-sectional view of nanocomposite films. The uniform distribution of the SNPs in the film can be clearly observed in the cross-sectional view of the FESEM images. The Fig. 2 (a, b, c, and d) shows the top view and cross section of the film. When the SNP nano-fillers are mixed with PU under ultrasound irradiation, with the increase in the concertation of the SNPs, more amount of SNPs will be dispersed in the PU film. The images are taken for the top view and cross section of the PU starch nanocomposite film. The cross-sectional view clearly shows that, with the increase in loading of starch nanoparticles (5 to 30 wt%, all right hand side images) in the PU matrix, more number of entanglement of SNPs occurs in PU due to enhanced shearing effect caused by the application of ultrasound irradiation.

The addition of nanoparticles induces additional molecular bonding and interaction in the PU polymer complex. These additional molecular interactions develop the higher mechanical and thermal properties in

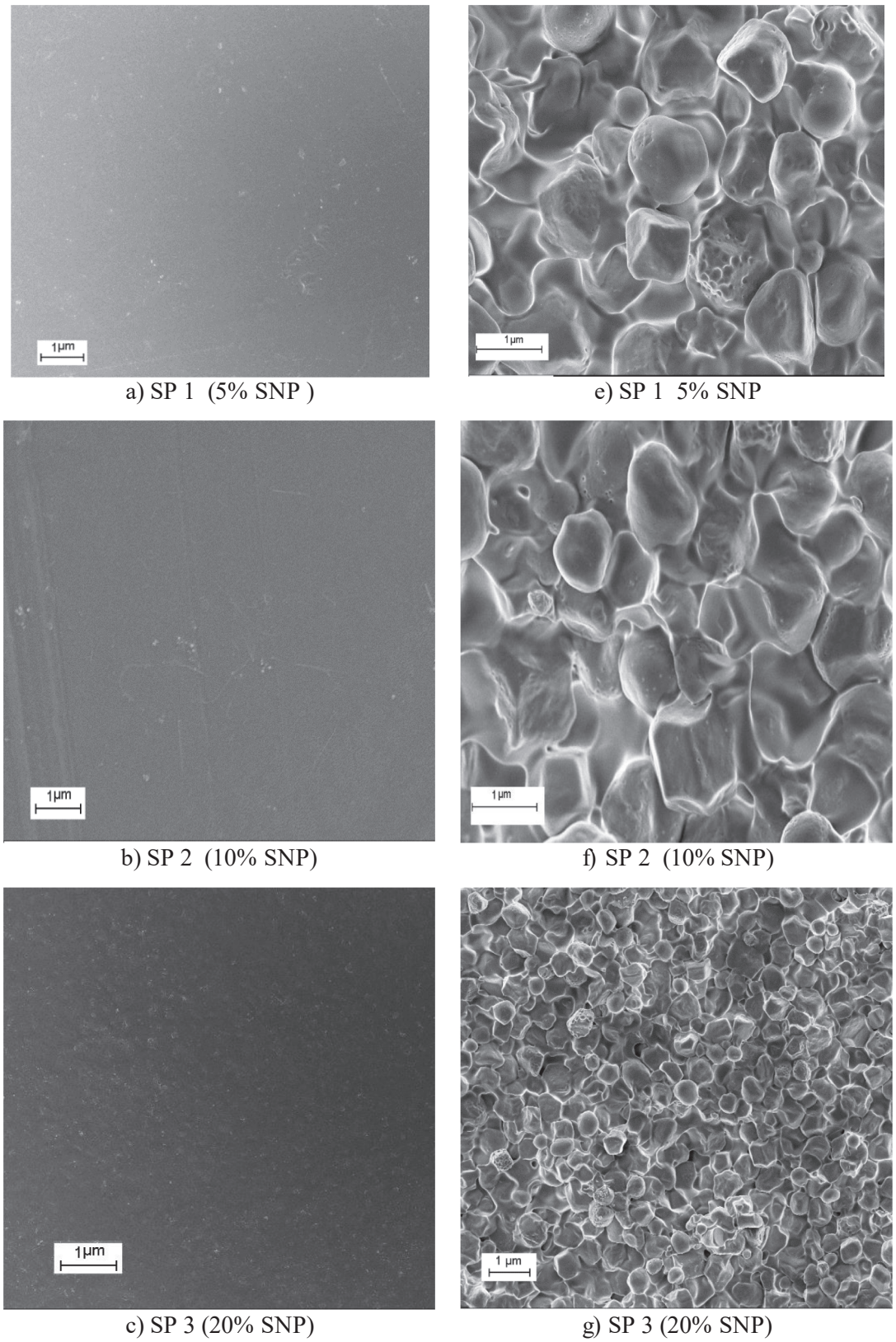

Fig. 2. FESEM images of films a) SP1, b) SP2, c) SP3, and d) SP4 are the surface microstructure views, and e) SP1, f) SP2, g) SP3, and h) SP4 are the cross-sectional view of film.

the nanocomposite films. The increase in the number of SNP per unit volume of polymer not only induces additional strength but also additional water and bacterial barrier to the PU matrix. The mechanical agitation is ineffective to achieve better dispersion over ultrasound assisted technique for SNP's loading in the PU matrix.

Several factors affect the homogeneity of the nanocomposite film

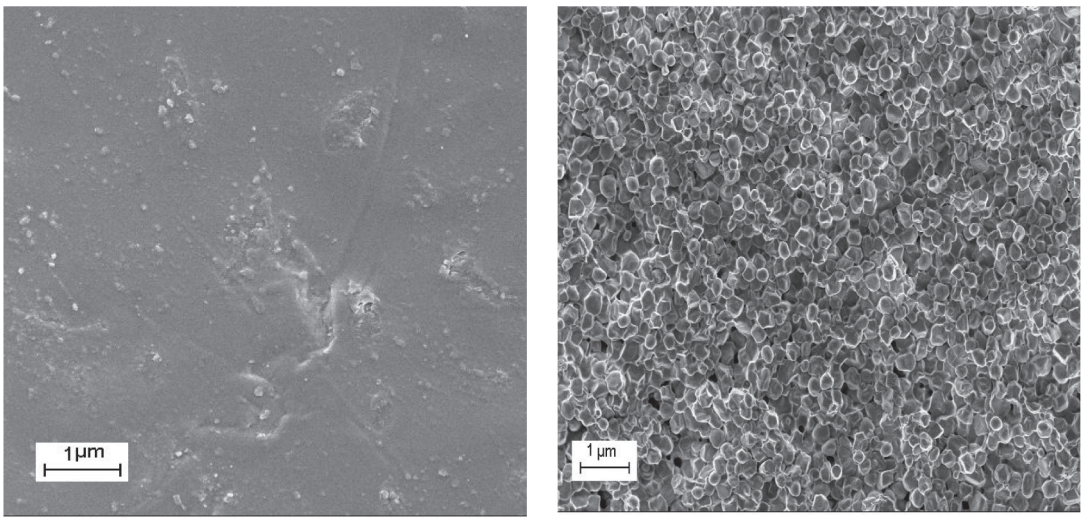

d) SP4 (30% SNP) h) SP4 30% SNP

Fig. 2. (*continued*).

[43]. Flocculation, coagulation, and clotting should be prevented during the homogenization of the SNP with the polymer matrix [44]. During the preparation of composites above 30% SNP additions, these phenomena are very common, thus the synthesized films show lumps of SNP, and uneven distribution across the film surface. The uneven distribution of SNP is a major issue due to which the strength, barrier properties, and thermal properties of nanocomposites can be affected [45].

3.2. Thermophysical properties of the SNP-PU nanocomposite film

DSC was used to investigate the molecular mixing of a SNP-PU matrix. Increased heat resistance was achieved by using a thermosetting polymer in conjunction with SNPs as a nanofiller in the PU polymer. The additon of SNP in PU results in a wide thermogram ranging from 64 °C to 93 °C. There had been no consistent molecular mixing of the components. Table 1 shows the effective Tg and melting point temperature (Tm) for the thin films of individual nanocomposite films. The significant difference in the Tg was observed for the nanocomposite film as the SNP concentration increased. The second-order transition temperature difference between the Tg and Tm rises by a few degrees, which significantly increases the processability of the polymer. At the 30% SNP addition, the difference between the two temperatures (Tm-Tg) is 42 °C, which is higher than the plan PU film (31 °C). This increase in the operating range of temperature at higher loading of the SNP will help to enhance the temperature resistance in the coating application.

The thermal decomposition of composite film was studied using a first derivative plot of weight % with respect to temperature. Fig. 3 illustrates the decomposition nature of different nanocomposite films against temperature.

The rise in the ΔH corresponds to the additional SNP mass in the polyurethane solution. The crystalline structure of the synthesized SNP blend with the PU solution develops the homogeneous suspension. The interaction between the surface activated SNP granules and the PU solution is the prominent reason behind the rise in the ΔH observed during the DSC of nanocomposite film. The rise in the ΔH occurs, when SNPs are added into the PU composite. The phenomena responsible for it is the local nucleation and crystallinity. Significant improvement in the crystallinity of SNP-PU matrix was observed at higher loading of SNPs i. e. the more number of polymeric changes are surrounded near the starch nanoparticles. This induces requirement of higher energy for the first phase change of SNP-PU nanocomposite polymer.

Table 1
DSC analysis of SNP-PU nanocomposites film.

	Film composition	Tg (°C)	Tm (°C)	ΔH (J g^{-1})
PU	100% PU	33.6	64.7	3.34
SP1	5% SNP + 95% PU	38.1	73.2	8.51
SP2	10% SNP + 90% PU	42.3	80.9	11.29
SP3	20% SNP + 80% PU	47.8	87.6	14.89
SP4	30% SNP + 70% PU	51.2	93.3	17.33

Fig. 2 shows that as the concentration of SNP in the PU solution increases, the compactness of the film increases significantly. The melting energy will be higher as the compactness of the film increases [46,47]. The presence of SNP requires a significant amount of enthalpy, Table 1 illustrates that, as with a 5% addition of SNP, the enthalpy rise is about 5 J g^{-1}. However, adding more SNP to PU solution results in significantly lower enthalpy values, which are around 3 J g^{-1} for each 10% SNP increase. The additional energy at an initial 5% SNP can be attributed to higher PU-SNP interaction. At lower concentrations of SNP, higher polymeric interaction requires more energy. At higher concentrations, SNP granules comes closer and thus the surface interaction increases. Table 2 shows that increasing the concentration of SNP in PU solution from zero to 5% increases the change in enthalpy per gm of nanocomposite film by 5 J. Furthermore, for a similar 10% rise in SNP concentration, the enthalpy change is 8 J per g.

Thermogravimetric analysis (TGA) and differential thermal analysis (DTA) of the thermoset composite thin sheets are shown in Fig. 3. TGA was carried out to understand the thermal stability and weight loss when increasing from room temperature to 800 °C at a rate of 10 °C min^{-1}. Initial weight loss was 10% for the pure PU thin sheet, which was observed to be below 100 °C due to the loss of volatile components present in the solution and moisture. A major weight loss of 40% occurred when the sample was heated from 200 to 300 °C. Both of the losses were due to the presence of low molecular weight components and amorphous components present in the PU. However, the addition of SNP to the PU solution shows higher resistance to degradation. The results show that the first weight loss of 10% in the SNP added thin composite sheets occurred at a temperature of 200 to 300 °C, which is much more than basic PU thin films. In this first stage of mass loss, observed due to the amount of moisture present in the thin sheet. As reported by Liu et al. [46] starch shows the first degradation at about 100 °C, whereas the second stage of degradation was observed around 350 °C. The SNP dispersed using US in the PU solution shows an additional energy requirement for the degradation of the complex with respect to virgin PU.

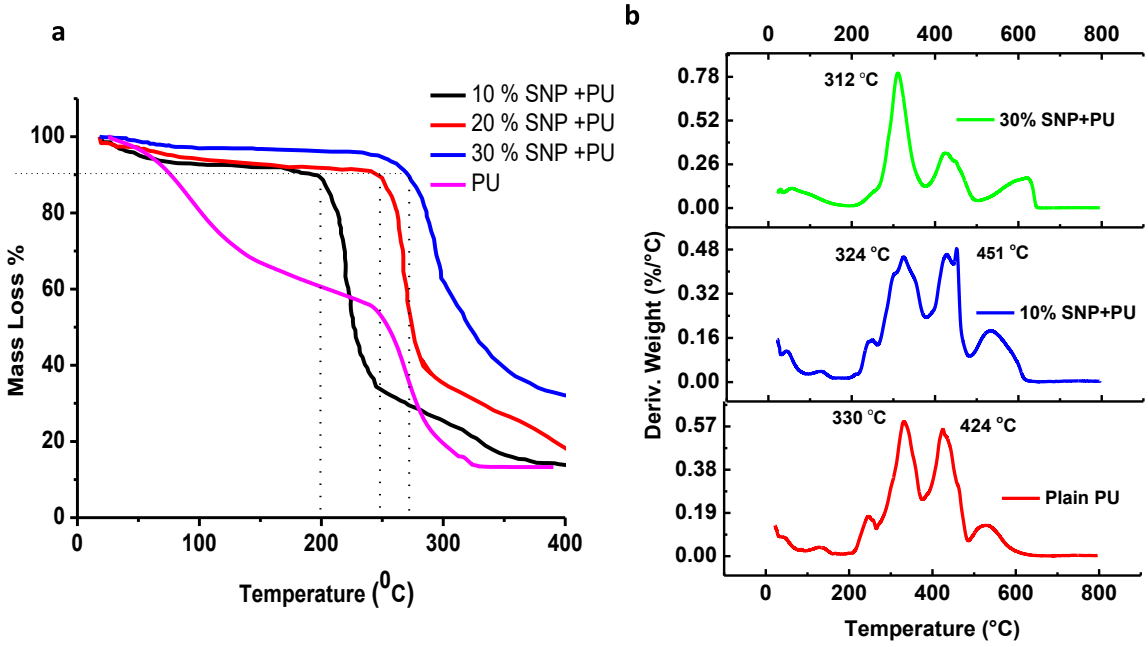

Fig. 3. Thermal degradation of the nanocomposite films with different composition of SNP and PU a) TGA and b) DTG.

Table 2
UV–Vis observations of the thin film.

Composition of nanocomposite thin film	Transmittance (T)	Absorbance (A)	Opacity of the thin film	Optical density of the thin film
PU	0.94	0.022	1.02	0.0086
5% SNP + PU	0.87	0.060	1.23	0.091
10% SNP + PU	0.73	0.137	2.91	0.464
20% SNP + PU	0.61	0.215	4.99	0.698
30% SNP + PU	0.53	0.276	5.87	0.768

As the weight percent of SNP in the PU solution increases, the resistance to thermal degradation also increases. The degradation window for the PU film was observed in between 100 and 300 °C. However, the SNP added nanocomposite shows higher degradation window which is starts from 200 °C to more than 400 °C. It could be possible that, addition of SNP in the polymer matrix develops an ionic bond with the PU components. These electrostatic bonds develop heat resistance in the nanocomposite thin sheets. The degradation rate of thin sheets decreases as the quantity of SNP added more. The uniform mixing of the SNP in the PU matrix substantially increases the thermal resistance of the film up to certain limitations. The Multistage decomposition DTG curves also favour the same conclusion as the TGA output of thermal analysis.

3.3. Mechanical strength analysis

The uniform mixing is the key feature to get the effective physical, mechanical and thermal strength to the film. These films show the various structural changes when they are exposed to external force. The uniform distribution of the SNPs for each composition helps to strengthen the film through the cross-section. The distribution of force applied on the PU film was divided into the starch granules which provides additional strength to the structure.

Fig. 4 shows the mechanical strength characteristics. Fig. 4 (a) gives the variation of tensile stress of the nanocomposite, whereas Fig. 4 (b) gives a clear idea of the flexural stress of nanocomposites. It can be found that as the concentration of nanofiller increases the TS resistance

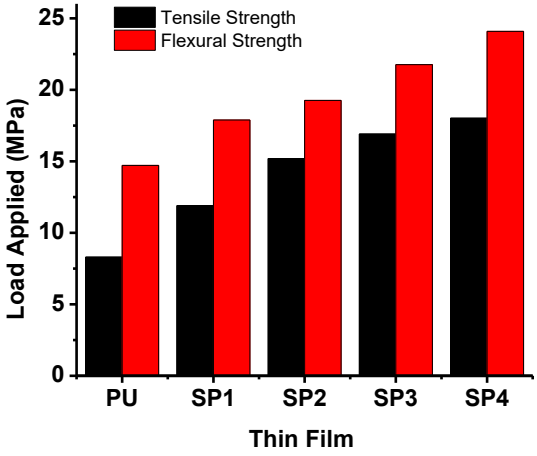

Fig. 4. Mechanical characteristics of nanocomposite films: a) tensile strength (MPa) and b) flexural strength (MPa).

and flexural stress resistance of nanocomposite films rise. However, at concentrations above the 25% SNP, the stress resistance decreased. This is because of the agglomeration of SNP nanofiller during the elongation, these agglomerated lumps provide additional repulsive forces to the PU matrix. This action of separation of SNP and PU reduces the overall value of TS as well as the flexural stress. The rise in the TS shows enhancement in the mechanical strength of PU films significantly. The crystalline nature of SNPs not only gives mechanical strength but also gives stiffness to the PU complex.

At the higher concentration of 30% SNP, the homogeneous SNP interactions within the matrix reduces the strength. As, the PU molecules' interaction with SNP overcomes the ultrasound irradiation energy the resultant rise in agglomeration rate of SNP is dominant. This leads to the formation of lumps SNP in the polymer matrix as seen in Fig. 2 (d) SP4 composition [47]. The lumps of SNP create the stress concentrated area across the polymer matrix under variable load. It can be observed in Fig. 5 that the percent elongation (%E) of nanocomposite films decreases as the SNP composition increases in the film. The crystalline nature of

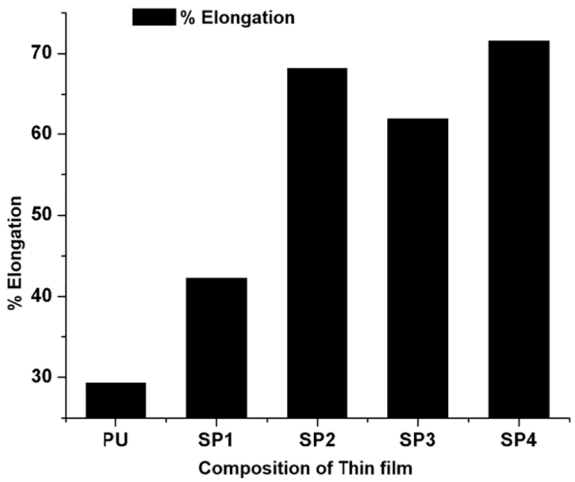

Fig. 5. Mechanical performance of different SNP compositional thin film.

the SNP produces stiffness in the PU film while, the interconnected bonds of the hydroxyl group and the sulphonic functional group offer rigidity to the PU matrix. The additional strength to the PU matrix shows significant variations in %E at lower applied forces. The results show that the bond developed due to hydroxyl functional group between PU and SNP will help the nanocomposite matrix to regain its shape and size up to Young's modulus of elasticity. The rise in %E with increasing SNP concentration implies the increased Young's modulus of elasticity with the higher SNP concentration until agglomeration starts. The enhancement in %E of nanocomposite film is also the function of uniform mixing, as it helps to avoid the agglomerated lumps of SNP in the polymer matrix. These lumps will generate the stress concentrated area at a particular location which will reduce the film capacity to regain its original shape and size. Thus, the ultimate %E value will be lower for the nanocomposite film. The uniformly distributed SNP nanofiller connects to the surrounding polymer matrix with a strong bond induced due to the hydroxyl functional group and provides additional strength against the externally applied force.

A significant increase in mechanical characteristics is seen when substantial thermal blending is carried out, with both the TS and %E increasing, resulting in the formation of toughened films. The %E of the films is in the range of 23 to 68% on average. When the films were subjected to vigorous mixing, it was discovered that the tensile qualities of the films were changed in a variety of ways. As a general rule, films with the highest proportion of TS also had the lowest rate of %E. From Fig. 5, it can be seen that when nanocomposite films are mixed intensively, they develop a significant degree of toughness as well as a high toughness-to-volume proportion.

The %E at the SP3 composition of SNP-PU nanocomposite shows lower value than that of SP4 in the Fig. 5. The reason behind it could be that the elongation phenomenon in the virgin PU corresponds to the effect of polymeric interactions, i.e., all the monomeric units are linked by strong covalent bonds and show corresponding elongation properties. The addition of SNP nanofiller will induce the directional secondary interactions in the SNP-PU polymer matrix, such as non-covalent bonds and hydrogen bonds. The overall %E of the SNP-PU nanocomposite film will be the cumulative effect of these intermolecular interactions. At lower concentrations of SNP, such as SP1 and SP2, the covalent bonds in the PU polymer complex will be dominant. However, at a higher concentration of SNP at SP4, the %E will be driven by the strength of directional secondary interactions of non-covalent bonds due to SNP nanofiller. At the critical concentration of SP3, the lower value of the %E in SNP-PU nanocomposite film will be due to a cumulative effect for which conventional covalent bonds and additional directional secondary interaction will be responsible [48].

3.4. Opacity of the SNP-PU thin film

Measurements of reflectance and transmittance over the visible spectrum are other important properties of these films. The opacity measurement is critical for packing items that are light sensitive. The ratio of light intensity that is incident on the surface of a thin film from a source to the fraction of light transmitted is defined as the opacity of the film. The transmitted portion of the light will depend on the film thickness and film composition. The resistance to direct transmission of light through the packaging film needs to be optimal enough to maintain the bacterial growth in the packed material, besides the visual appearance. The optimal value of nanofillers is dependent on the required optical density for the packed material.

Transmittance value at a wavelength of 600 nm was noted for the different compositions of SNP-PU nanocomposite film. The baseline comparison was carried out with virgin PU thin film. The observed values of transmittance show a gradual decrease with an increase in SNP composition in the nanocomposite film. This decrease in the transmittance was due to the addition of crystalline SNP to the PU complex. The strong crystalline structure of SNP induces resistance to light traveling through the film. The portion of light incident on the crystalline structure was reflected that was recorded. This reflection increases as the number of SNP increases in the fixed surface area of the thin film, which is nevertheless the concentration of SNP. The optical density of the film is calculated by, $\text{Optical Density} = \text{Log}_{10}(\text{Opacity})$. Table 2 shows that as the SNP concentration increases, the optical density of the film decreases significantly. As the increase in compactness of the film with SNP concentration results in a rise in optical density. The observations show clearly that, with the addition of 5% SNP in pure PU complex, the rise in optical density was about 9%, whereas, with the addition of 10% SNP, it was 46%. The rise in SNP by 20% and 30% show a rise in optical density of 69% and 76%, respectively. The relative increase from 5% to 10% SNP was significant as it showed an 80% rise in optical density. However, addition above 10% SNP enhances the optical density by 33% and 9%, respectively, for 20% and 30% SNP addition.

3.5. Bacterial barrier property analysis of nanocomposite films

The diluted culture after the absorption study was placed on the agar plate to measure the bacterial count. The number of bacteria growing on each plate was determined as discussed in the experimental section, and the total bacterial count in each flask was calculated. The absorbance at 600 nm of the cultures in conical flasks after exposure to the environment was measured and the results are shown in Fig. 6. The absorbance values were high in the control flask when compared to the flasks sealed with polyurethane films. Though the results were conclusive, we still determined the bacterial count by serial dilution and plating. This might

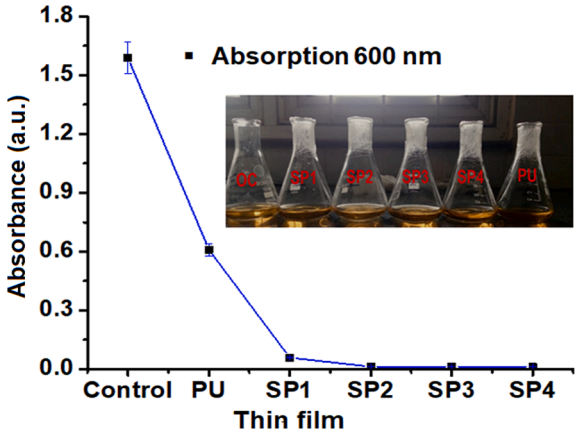

Fig. 6. Bacterial density using UV spectroscopy.

be due to the fact that the flasks sealed with polyurethane film allow bacteria to pass through them while the SNP-PU composite films filter the bacteria present in the external environment. Although the polyurethane film closed flask had bacterial growth, the bacterial count was significantly less than the control. It was found that the control flask had a high bacterial count of 5×10^9, whereas the flask sealed with PU films had a bacterial count of 2.5×10^3. The conical flasks sealed with SP1, SP2, SP3, and SP4 did not have any bacteria growing in them.

The commonly found E. coli was used for the experiments. The size of E. coli varied from 1.0 to 2.0 μm in length with a radius of about 0.5 μm [49]. However, the pore size of virgin PU synthesised by the casting method was reported to be between 50 and 100 μm [50]. From the experimental results, it can be concluded that ultrasonically dispersed SNP gets occupied in the pore of the PU complex. The uniform distribution of SNP in the PU solution reduces the overall pore size of nanocomposite thin film. This phenomenon of nanofilling helps to develop resistance to bacterial as well as air passages through the thin sheet.

The compact structures of the film were attributed to the ultrasonic irradiation during the blending of the SNP and PU. The rate of transmission of bacteria across the film from a bacteria-rich environment to a closed culture inside the flask decreased due to the narrower pore openings at the surface of the nanocomposite film [51,52]. The nanocomposite film shows higher resistance to even 24 h of continuous environmental exposure. Thus, bacterial resistance at the lower additional SNP in the PU matrix is positive for its packaging application. This again shows that the polyurethane films have the ability to filter microorganisms from the external environment, but the efficiency is far less than the SP films.

3.6. Barrier performance of nanocomposite thin film.

3.6.1. Water vapour permeability (WVP).

The transmission rate of water vapour through the micropores of the thin film is significant for packaging applications. The average 50 μm thick thin film with a 78.54 cm2 area was used for the experiments. The observed results are shown in Fig. 7. The SNP was added uniformly in the PU complex producing a uniform PU-SNP film structure. The WVP varies with the surrounding temperatures and concentration of SNP in nanocomposite film. From Fig. 2, it was clear that as the SNP density increases the compactness in the composite film also increases. This phenomenon reduces the pore size of SNP-PU composite film due to which the rate of transmission of vapours across the thickness of film reduces. The travel time of water vapours increases as the thickness of the film increases. At the higher thickness, the diffusion of water vapor across the plane of the film may also be the reason for the reduction of WVP across the film.

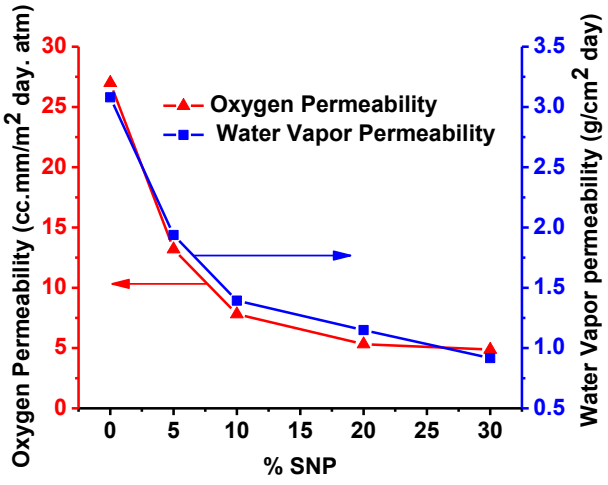

Fig. 7. Water vapour and oxygen barrier performance of composite thin film.

Another important parameter is the surrounding temperature. The rise in the temperature directly affects the gross humidity across the film. The humidity difference leads to the higher pressure gradient across the film which is the reason for the higher WVP. The observations from the experiments indicate that at the higher temperature the WVP increases. The higher concentration of SNP (30%) shows the lowest WVP about 0.917 g pa^{-1} cm^{-2} day^{-1}, which is again increasing at higher temperatures. This may cause a higher diffusion rate of water vapor across the thin film at higher temperatures above 35 °C. At higher temperatures, the vapor pressure is overcome by the static pressure leading to a higher pressure drop across the film. The relative humidity inside the vessel increases with the rise in the temperature. The higher difference in relative humidity across the film was the driving force for the higher molecular transformation. Similar results for the starch glycerol films were reported by Miranda et al. [53]. The film with the addition of 20% concentration of SNP shows an effective reduction of 60% WVP and above. At higher addition of SNP in the polymer complex, the formation of lumps was detected.

3.6.2. Oxygen barrier of nanocomposite thin film.

Fig. 7 illustrates the effect of SNP concentration enhancement in the nanocomposite complex for the water vapor and oxygen transmission through the thin film. The specimen used for the analysis was with a uniform thickness of 200 μm. The synthesized thin film with the specific (dia. 50 mm) dimension was placed. The transmission rate of oxygen was reduced as the % SNP increased in the composite film. The addition of 5% SNP in the composite thin film shows the drastic reduction in oxygen permeability. The results observed from the experiments show 44% reduction in oxygen permeability with the addition of 5% SNP. However, the permeability reduction rate was reduced after 5% SNP. With the addition of 10% SNP, a permeability reduction of 65% was observed. The reduction of 75% and 84% were observed with the addition of 20% and 30% SNP respectively. The uniform distribution of SNP in the PU matrix will reduce the pore size at the lowest stage, this will make thin-film most impermeable.

The synthesized nanocomposite SNP-PU films shows a lower operating stress zone between tensile stress and flexural stress. The effective reduction in WVP to 60 to 85%, makes the film valuable for packaging applications at lower temperature conditions. At lower temperatures up to 40 °C, the film shows higher thermal stability, resistance against bacterial (99%), water vapor transformation and higher mechanical properties make it suitable as a packaging material. The extent of acid hydrolysis with ultrasound assistance was enhanced significantly in the starch granules during the synthesis of SNP. The process is robust and produces a batch of SNPs with a nanoscale size. The SNP-based PU nanocomposite thin film shows enhanced mechanical and thermal moisture barrier performance. These films exhibit higher resistivity to water vapour and oxygen permeability. Further, there is a significant improvement in the resistance to bacterial transmission through nanocomposite films, which find prominent applicability in food packaging.

4. Conclusions

The synthesis of uniform distribution of starch nanoparticles in PU was achieved with ultrasound assistance. The rise in the concentration of starch nanofiller in the PU matrix enhanced the mechanical and thermal properties of the thin film. Ultrasound assisted acid hydrolysis showed lower particle size of SNPs compared to conventional synthesis process, hence there is improved performance due to increase in the local crystallinity. The synthesized nanocomposite films show 99% resistance to bacterial transformation. The optimal value of the SNP to achieve the maximum bacterial transformation resistance is 5%. The glass transition temperature of nanocomposite films shows an increasing pattern as the percentage of SNP increases in the PU complex. The increase in the glass transition temperature is due to increase in the overall

crystallinity imparted by uniform dispersion of starch nanoparticles in the PU matrix. The uniform distribution of SNP in the polymer complex reduces the pore size of the film surface as compared to the plan PU film. The water vapour permeability (WVP) of the film was affected by the temperature of the surroundings and the concentration of SNPs in the film. Overall with the addition of 20% SNP, the WVP was reduced to 60%, whereas oxygen permeability was reduced to 75%. The opacity of the film decreased as the SNP concentration increased, the film became more rigid, and the flexural stress of the thin film showed a reduction with a rise in SNP concentration. The tensile strength of the film was increased by the addition of SNP which implies the rise in young's modulus of the film. At lower temperatures up to 40 °C, the prepared SNP-PU nanocomposite film showed higher thermal stability, resistance against bacterial, water vapour transformation, and higher mechanical properties making it suitable as a packaging material.

Declaration of Competing Interest

The authors declare that they have no known competing financial interests or personal relationships that could have appeared to influence the work reported in this paper.

Acknowledgment

Authors acknowledge to Ministry of Science and Technology India, Department of Science and Technology international bilateral cooperation division, for financial assistance through Indo Tunisia Project grant no DST/INT/TUNISIA/P-06/2017. The authors are also grateful to Conselho Nacional de Desenvolvimento Científico e Tecnológico (CNPq, Grant 309297/2016-8), Instituto Nacional de Ciência e Tecnologia de Bioanalítica – INCTBio (CNPq Grant Nr. 573672/2008-3) and Fundação de Amparo à Pesquisa do Estado do Rio Grande do Sul (FAPERGS, Grant 16/2551-0000516-8).

References

[1] S.S. Low, C.N. Lim, M. Yew, W.S. Chai, L.E. Low, S. Manickam, B.T. Tey, P.L. Show, Recent ultrasound advancements for the manipulation of nanobiomaterials and nanoformulations for drug delivery, Ultrason. Sonochem. 80 (2021), 105805, https://doi.org/10.1016/j.ultsonch.2021.105805.

[2] L.A. Castillo, S. Farenzena, E. Pintos, M.S. Rodríguez, M.A. Villar, M.A. García, O. V. López, Active films based on thermoplastic corn starch and chitosan oligomer for food packaging applications, Food Packag. Shelf, Life. 14 (2017) 128–136, https://doi.org/10.1016/j.fpsl.2017.10.004.

[3] J.H. Jagannath, C. Nanjappa, D.K. Das Gupta, A.S. Bawa, Mechanical and barrier properties of edible starch-protein-based films, J. Appl. Polym. Sci. 88 (2003) 64–71, https://doi.org/10.1002/app.11602.

[4] M. Tajik, H.J. Torshizi, H. Resalati, Y. Hamzeh, Effects of cationic starch in the presence of cellulose nanofibrils on structural, optical and strength properties of paper from soda bagasse pulp, Carbohydr. Polym. 194 (2018) 1–8, https://doi.org/10.1016/j.carbpol.2018.04.026.

[5] H. Tian, J. Yan, A.V. Rajulu, A. Xiang, X. Luo, Fabrication and properties of polyvinyl alcohol/starch blend films: Effect of composition and humidity, Int. J. Biol. Macromol. 96 (2017) 518–523, https://doi.org/10.1016/j.ijbiomac.2016.12.067.

[6] S. Mali, M.V.E. Grossmann, M.A. García, M.N. Martino, N.E. Zaritzky, Effects of controlled storage on thermal, mechanical and barrier properties of plasticized films from different starch sources, J. Food Eng. 75 (2006) 453–460, https://doi.org/10.1016/j.jfoodeng.2005.04.031.

[7] L. Dai, C. Qiu, L. Xiong, Q. Sun, Characterisation of corn starch-based films reinforced with taro starch nanoparticles, Food Chem. 174 (2015) 82–88, https://doi.org/10.1016/j.foodchem.2014.11.005.

[10] N. Zheng, L. Wang, Z. Sun, The effects of ultrasonication power and time on the dispersion stability of few-layer graphene nanofluids under the constant ultrasonic energy consumption condition, Ultrason. Sonochem. 80 (2021), 105816, https://doi.org/10.1016/j.ultsonch.2021.105816.

[11] E.A. Alenyorege, H. Ma, I. Ayim, F. Lu, C. Zhou, Efficacy of sweep ultrasound on natural microbiota reduction and quality preservation of Chinese cabbage during storage, Ultrason. Sonochem. 59 (2019), 104712, https://doi.org/10.1016/j.ultsonch.2019.104712.

[12] A. Inui, A. Honda, S. Yamanaka, T. Ikeno, K. Yamamoto, Effect of ultrasonic frequency and surfactant addition on microcapsule destruction, Ultrason. Sonochem. 70 (2021), 105308, https://doi.org/10.1016/j.ultsonch.2020.105308.

[13] S. Bel Haaj, A. Magnin, C. Petrier, S. Boufi, Starch nanoparticles formation via high power ultrasonication, Carbohydr. Polym. 92 (2013) 1625–1632, https://doi.org/10.1016/j.carbpol.2012.11.022.

[14] L. Zhou, X. He, N. Ji, L. Dai, Y. Li, J. Yang, L. Xiong, Q. Sun, Preparation and characterization of waxy maize starch nanoparticles via hydrochloric acid vapor hydrolysis combined with ultrasonication treatment, Ultrason. Sonochem. 80 (2021), https://doi.org/10.1016/j.ultsonch.2021.105836.

[15] M. Girard, F. Bertrand, J.R. Tavares, M.-C. Heuzey, Rheological insights on the evolution of sonicated cellulose nanocrystal dispersions, Ultrason. Sonochem. 78 (2021), 105747, https://doi.org/10.1016/j.ultsonch.2021.105747.

[16] S. Sumitomo, H. Koizumi, M.A. Uddin, Y. Kato, Comparison of dispersion behavior of agglomerated particles in liquid between ultrasonic irradiation and mechanical stirring, Ultrason. Sonochem. 40 (2018) 822–831, https://doi.org/10.1016/j.ultsonch.2017.08.023.

[17] E.A. Serna-Galvis, J.F. Guateque-Londoño, J. Silva-Agredo, J. Porras, Y. Ávila-Torres, R.A. Torres-Palma, Superior selectivity of high-frequency ultrasound toward chorine containing-pharmaceuticals elimination in urine: A comparative study with other oxidation processes through the elucidation of the degradation pathways, Ultrason. Sonochem. 80 (2021), https://doi.org/10.1016/j.ultsonch.2021.105814.

[18] S. Kalia, A. Dufresne, B.M. Cherian, B.S. Kaith, L. Avérous, J. Njuguna, E. Nassiopoulos, Cellulose-based bio- and nanocomposites: A review, Int. J. Polym. Sci. 2011 (2011), https://doi.org/10.1155/2011/837875.

[19] P. Kampeerapappun, D. Aht-ong, D. Pentrakoon, K. Srikulkit, Preparation of cassava starch/montmorillonite composite film, Carbohydr. Polym. 67 (2007) 155–163, https://doi.org/10.1016/j.carbpol.2006.05.012.

[20] P.G. Seligra, C. Medina Jaramillo, L. Famá, S. Goyanes, Biodegradable and non-retrogradable eco-films based on starch-glycerol with citric acid as crosslinking agent, Carbohydr. Polym. 138 (2016) 66–74, https://doi.org/10.1016/j.carbpol.2015.11.041.

[21] H. Dai, P.R. Chang, F. Geng, J. Yu, X. Ma, Preparation and properties of starch-based film using N, N-bis(2-hydroxyethyl)formamide as a new plasticizer, Carbohydr. Polym. 79 (2010) 306–311, https://doi.org/10.1016/j.carbpol.2009.08.012.

[22] M.C. Galdeano, S. Mali, M.V.E. Grossmann, F. Yamashita, M.A. García, Effects of plasticizers on the properties of oat starch films, Mater. Sci. Eng. C. 29 (2009) 532–538, https://doi.org/10.1016/j.msec.2008.09.034.

[23] A.S. Abreu, M. Oliveira, A. De Sá, R.M. Rodrigues, M.A. Cerqueira, A.A. Vicente, A. V. Machado, Antimicrobial nanostructured starch based films for packaging, Carbohydr. Polym. 129 (2015), https://doi.org/10.1016/j.carbpol.2015.04.021.

[24] H. Angellier, S. Molina-Boisseau, A. Dufresne, Mechanical properties of waxy maize starch nanocrystal reinforced natural rubber, Macromolecules. 38 (2005) 9161–9170, https://doi.org/10.1021/ma0512399.

[25] B.B. Sanchez de la Concha, E. Agama-Acevedo, M.C. Nunez-Santiago, L.A. Bello-Perez, H.S. Garcia, J. Alvarez-ramirez, Acid hydrolysis of waxy starches with different granule size for nanocrystal production, J. Cereal Sci. 79 (2018) 193–200, https://doi.org/10.1016/j.jcs.2017.10.018.

[26] P. Liu, W. Gao, X. Zhang, B. Wang, F. Zou, B. Yu, L. Lu, Y. Fang, Z. Wu, C. Yuan, B. Cui, Effects of ultrasonication on the properties of maize starch/stearic acid/sodium carboxymethyl cellulose composite film, Ultrason. Sonochem. 72 (2021), https://doi.org/10.1016/j.ultsonch.2020.105447.

[27] Y. Shen, J. He, Z. Xie, X. Zhou, C. Fang, C. Zhang, Synthesis and characterization of vegetable oil based polyurethanes with tunable thermomechanical performance, Ind. Crops Prod. 140 (2019), https://doi.org/10.1016/j.indcrop.2019.111711.

[28] C.S. Wong, N.I. Hassan, M. Sukor, M.A.P. Serra, J. Alberto, M. Gonzalez, L. Angel, K. Haji, Photo-activated self-healing bio-based polyurethanes, Ind. Crop. Prod. 140 (2019), 111613, https://doi.org/10.1016/j.indcrop.2019.111613.

[29] J. Chen, Q. Wang, M. Luan, J. Mo, Y. Yan, X. Li, Polydopamine as reinforcement in the coating of nano-silver on polyurethane surface: Performance and mechanisms, Prog. Org. Coatings. 137 (2019), https://doi.org/10.1016/j.porgcoat.2019.105288.

[30] M.E.V. Hormaiztegui, B. Daga, M.I. Aranguren, V. Mucci, Bio-based waterborne polyurethanes reinforced with cellulose nanocrystals as coating films, Prog. Org. Coatings. 144 (2020), 105649, https://doi.org/10.1016/j.porgcoat.2020.105649.

[31] H.-C. Zhang, B. Kang, L.-S. Chen, X. Lu, Enhancing toughness of poly (lactic acid)/Thermoplastic polyurethane blends via increasing interface compatibility by polyurethane elastomer prepolymer and its toughening mechanism, Polym. Test. 87 (2020), 106521, https://doi.org/10.1016/j.polymertesting.2020.106521.

[32] H. Zhang, Y. She, S. Song, H. Chen, J. Pu, Improvements of mechanical properties and specular gloss of polyurethane by modified nanocrystalline cellulose, BioResources. 7 (2012) 5190–5199. 10.15376/biores.7.4.5190-5199.

[33] Y. Lu, L. Tighzert, F. Berzin, S. Rondot, Innovative plasticized starch films modified with waterborne polyurethane from renewable resources, Carbohydr. Polym. 61 (2005) 174–182, https://doi.org/10.1016/j.carbpol.2005.04.013.

[34] M. Yazdi, V. Haddadi Asl, M. Pourmohammadi, H. Roghani-Mamaqani, Mechanical properties, crystallinity, and self-nucleation of carbon nanotube-polyurethane nanocomposites, Polym. Test. 79 (2019), 106011, https://doi.org/10.1016/j.polymertesting.2019.106011.

[35] V.S. Hakke, U.D. Bagale, S. Boufi, G.U.B. Babu, S.H. Sonawane, Ultrasound Assisted Synthesis of Starch Nanocrystals and It's Applications with Polyurethane for Packaging Film, J. Renew. Mater. 08 (2020) 239–250. 10.32604/jrm.2020.08449.

[36] A.P. Bonto, R.N. Tiozon, N. Sreenivasulu, D.H. Camacho, Impact of ultrasonic treatment on rice starch and grain functional properties: A review, Ultrason. Sonochem. 71 (2021) 105383.

[37] S. Boufi, S. Bel Haaj, A. Magnin, F. Pignon, M. Impéror-Clerc, G. Mortha, Ultrasonic assisted production of starch nanoparticles: Structural characterization and

mechanism of disintegration, Ultrason. Sonochem. 41 (2018) 327–336, https://doi.org/10.1016/j.ultsonch.2017.09.033.
[38] C.A. International, S.T. Method, Standard Test Method for Tensile Properties of Thin Plastic Sheeting, ASTM. 08 (01) (2017) 9, https://doi.org/10.1520/D0882-00.
[39] C.A. International, S.T. Method, Standard Test Method for Oxygen Gas Transmission Rate Through Plastic Film and Sheeting Using a Coulometric Sensor, Cell. 15.10 (2017) 7. 0.1520/D3985-17.
[40] W.K. Lewis, W.G. Whitman, Principles of Gas Absorption, Ind. Eng. Chem. 16 (1924) 1215–1220, https://doi.org/10.1021/ie50180a002.
[41] R. Chang, N. Ji, M. Li, L. Qiu, C. Sun, X. Bian, H. Qiu, L. Xiong, Q. Sun, Green preparation and characterization of starch nanoparticles using a vacuum cold plasma process combined with ultrasonication treatment, Ultrason. Sonochem. 58 (2019), https://doi.org/10.1016/j.ultsonch.2019.104660.
[42] L. Dai, C. Li, J. Zhang, F. Cheng, Preparation and characterization of starch nanocrystals combining ball milling with acid hydrolysis, Carbohydr. Polym. 180 (2018), https://doi.org/10.1016/j.carbpol.2017.10.015.
[43] Z. Cherifi, B. Boukoussa, A. Zaoui, M. Belbachir, R. Meghabar, Structural, morphological and thermal properties of nanocomposites poly(GMA)/clay prepared by ultrasound and in-situ polymerization, Ultrason. Sonochem. 48 (2018) 188–198, https://doi.org/10.1016/j.ultsonch.2018.05.027.
[44] R. Kumar, G. Ghoshal, M. Goyal, Synthesis and functional properties of gelatin/CA–starch composite film: excellent food packaging material, J. Food Sci. Technol. 56 (2019) 1954–1965, https://doi.org/10.1007/s13197-019-03662-4.
[45] S.M. Noorbakhsh-Soltani, M.M. Zerafat, S. Sabbaghi, A comparative study of gelatin and starch-based nano-composite films modified by nano-cellulose and chitosan for food packaging applications, Carbohydrate Polymers 189 (2018) 48–55.
[46] Y. Liu, L. Yang, C. Ma, Y. Zhang, Thermal behavior of sweet potato starch by non-isothermal thermogravimetric analysis, Materials (Basel). 12 (2019), https://doi.org/10.3390/ma12050699.
[47] J. Li, Y. Li, Y. Song, S. Niu, N. Li, Ultrasonic-assisted synthesis of polyvinyl alcohol/phytic acid polymer film and its thermal stability, mechanical properties and surface resistivity, Ultrason. Sonochem. 39 (2017) 853–862, https://doi.org/10.1016/j.ultsonch.2017.06.017.
[48] A. Kulshreshtha, K.J. Modica, A. Jayaraman, Impact of Hydrogen Bonding Interactions on Graft-Matrix Wetting and Structure in Polymer Nanocomposites, Macromolecules. 52 (2019) 2725–2735, https://doi.org/10.1021/acs.macromol.8b02666.
[49] N. Hilal, V. Kochkodan, L. Al-Khatib, T. Levadna, Surface modified polymeric membranes to reduce (bio)fouling: A microbiological study using E. coli, Desalination. 167 (2004) 293–300, https://doi.org/10.1016/j.desal.2004.06.138.
[50] M. Nayani, S. Gunashekar, N. Abu-Zahra, Synthesis and characterization of polyurethane-nanoclay composites, Int. J. Polym. Sci. 2013 (2013) 1–5, https://doi.org/10.1155/2013/717895.
[51] S.A. Madbouly, Waterborne Polyurethane Dispersions and Thin Films : Biodegradation and Antimicrobial Behaviors, Molecules. 26 (2021) 961.
[52] B. Sukkaneewat, S. Utara, Ultrasonic-assisted Dunlop method for natural rubber latex foam production: Effects of irradiation time on morphology and physico-mechanical properties of the foam, Ultrason. Sonochem. 82 (2022), 105873, https://doi.org/10.1016/j.ultsonch.2021.105873.
[53] C.S. Miranda, M.S. Ferreira, M.T. Magalhães, A.P.G. Bispo, J.C. Oliveira, J.B. A. Silva, N.M. José, Starch-based Films Plasticized with Glycerol and Lignin from Piassava Fiber Reinforced with Nanocrystals from Eucalyptus, Mater. Today Proc. 2 (2015) 134–140, https://doi.org/10.1016/j.matpr.2015.04.038.

Further reading

[8] S.S. Low, M. Yew, C.N. Lim, W.S. Chai, L.E. Low, S. Manickam, B.T. Tey, P.L. Show, Sonoproduction of nanobiomaterials – A critical review, Ultrason. Sonochem. 82 (2022), 105887, https://doi.org/10.1016/j.ultsonch.2021.105887.
[9] A. Rahaman, A. Kumari, X.A. Zeng, M. Adil Farooq, R. Siddique, I. Khalifa, A. Siddeeg, M. Ali, M. Faisal Manzoor, Ultrasound based modification and structural-functional analysis of corn and cassava starch, Ultrason. Sonochem. 80 (2021) 105795. 10.1016/j.ultsonch.2021.105795.